ACS OMEGA

http://pubs.acs.org/journal/acsodf

Article

# DNA-Immobilized Fluorescent Polystyrene Nanoparticles as Probes with Tunable Detection Limits

Jin Sol Shin and Sheng Li*

Cite This: *ACS Omega* 2022, 7, 48310−48319

Read Online

ACCESS | Metrics & More | Article Recommendations | Supporting Information

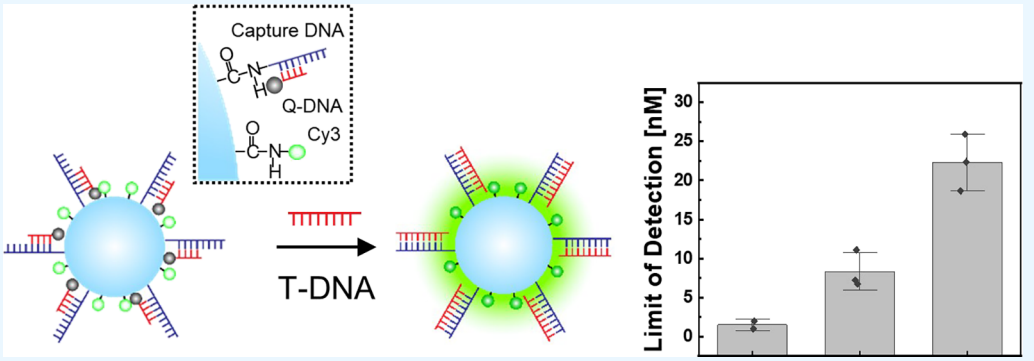


**ABSTRACT:** DNA-immobilized nanoparticle probes show high target specificity; thus, they are employed in various bioengineering and biomedicine applications. When the nanoparticles employed are dye-loaded polymer particles, the resulting probes have the additional benefit of biocompatibility and versatile surface properties. In this study, we construct DNA-immobilized fluorescent polystyrene (PS) nanoparticles through controlled surface reactions. PS nanoparticles with surface carboxyl groups are utilized, and amine-functionalized dye molecules and capture DNAs are covalently immobilized via a one-pot reaction. We show that the surface chemistry employed allows for quantitative control over the number of fluorescent dyes and DNA strands immobilized on the PS nanoparticle surfaces. The nanoparticles thus prepared are then used for DNA detection. The off state of the nanoprobe is achieved by hybridizing quencher-functionalized DNAs (Q-DNAs) to the capture DNAs immobilized on nanoparticle surfaces. Target-DNAs (T-DNAs) are detected by the displacement of the prehybridized Q-DNAs. The nanoprobes show successful detection of T-DNAs with high sequence specificity and long-term stability. They also show excellent detection sensitivity, and the detection limit can be tuned by adjusting the capture DNA-to-dye ratio.

## INTRODUCTION

Nucleic acid (NA)-based detection technologies are widely used in bioengineering and biomedicine applications due to the high sensitivity and specificity of nucleotide base pairing.[1,2] While NA detection in both solution-based[3−5] and surface-based systems[6−8] have been illustrated, the latter has the advantage of reduced separation processes, elimination of pre-preparation steps, and non-requirement of sophisticated instrumentation.[9,10] In particular, when the substrates used for capture NA immobilization are nanoparticles, improvement in detection sensitivity has been reported.[11,12] In early studies, inorganic gold,[13−15] silica,[16] and silver nanoparticles[17] are commonly employed. For example, Mirkin's group developed probes termed nano-flares, which were constructed by hybridizing fluorophore-labeled reporter sequences with NA-immobilized gold nanoparticles.[15] The target NAs were detected via strand displacement of the reporter sequences, leading to quantitative detection with high fluorescent signaling. Recently, fluorescent nanoparticles, including quantum dots[18] and dye-doped silica particles,[19−21] have been utilized to serve the dual function of emission centers and solid substrates for NA immobilization. In one example, Liu et al. prepared nanosensors by immobilizing fullerene-labeled molecular beacons on quantum dots.[18] In combination with the use of magnetic particles as carriers, the system exhibited rapid detection time and low detection limits. Although the inorganic nanoparticle-based sensors show good detection performance, they commonly suffer from cytotoxicity related issues and thus have limited use for in vivo applications.[22−24]

To overcome the shortcomings associated with inorganic nanoparticles, organic fluorescent probes,[25,26] including dye-loaded polymer nanoparticles, present themselves as attractive alternatives. Dye-loaded polymer nanoparticles have been

Received: October 9, 2022
Accepted: November 30, 2022
Published: December 15, 2022

demonstrated as contrast agents for bio-imaging applications due to low cytotoxicity and high enzyme resistance;[27−29] thus, their utilization as substrates for NA immobilization is expected to lead to sensors with enhanced biocompatibility. The polymer nanoparticles are also considered to have more design flexibility than the inorganic nanoparticles.[30,31] The fluorescence of dye-loaded polymer nanoparticles may be tuned by varying both the particle size and the concentration of the dyes loaded. In contrast, the emission properties of many inorganic nanoparticles are intrinsically coupled to the particle sizes and thus cannot be tuned independently. Moreover, the surface properties of the polymer nanoparticles may be easily manipulated through the chemical incorporation of functional groups, but such surface modification is harder to achieve for inorganic particles.[21,32] Despite the many advantages, reports on polymer nanoparticle-based NA sensors remain limited. Melnychuk and Klymchenko prepared highly bright dye-loaded poly(methyl methacrylate-*co*-methacrylic acid) nanoparticles then immobilized capture DNA sequences on the nanoparticle surfaces.[10] The resulting nanoprobes showed outstanding brightness and amplification characteristics, leading to the detection of target DNA sequences with a low detection limit. Stawicki et al. also reported fluorescent polymer nanoparticles for peptide and protein detection.[33] In this case, commercially available dye-loaded polystyrene (PS) nanoparticles were used. The nanoparticles were surface modified with polyethylene glycol and then immobilized with DNA aptamers via linker molecules.

The dye-loaded polymer nanoparticles reported thus far are commonly prepared by nanoprecipitation.[28,29,34] In this process, polymers are combined with dye molecules and the mixture is then co-precipitated to form dye-loaded nanoparticles.[35,36] As the dye encapsulation process is kinetically controlled, fine-tuning the number of dyes incorporated can be difficult. Additionally, as the dyes are not covalently bound to the nanoparticles, the elution of the dye over time may also be of potential concern. Surface immobilization of small and large organic molecules via covalent bond formation is widely employed to modify the properties of polymer particles.[32,33,37] We envision that the same type of surface reactions can be extended to prepare NA probes with improved tunability and stability. In this study, we utilize PS nanoparticles with surface carboxyl functional groups then immobilize amine-functionalized dye molecules and capture DNAs. The off state of the nanoprobe is achieved by the hybridization of quencher-functionalized DNA (Q-DNA) to capture DNA, and target DNA (T-DNA) detection is then achieved through a simple strand displacement strategy (Scheme 1). The chemistry employed allows for quantitative control over the number of fluorescent dyes and DNA strands immobilized on PS surfaces, leading to nanoprobes with high sensitivity and long-term stability. The prepared nanoprobes have the additional advantage of displaying a tunable detection limit, which is achieved by adjusting the capture DNA-to-dye ratio.

## EXPERIMENTAL SECTION

**Materials.** HPLC-purified single-stranded DNA sequences were purchased from Bioneer, dissolved in triple distilled water (TDW), aliquoted, and stored at −20 °C for further experiment. The oligonucleotide sequences used in this study are shown below. Amine-functionalized capture DNA (amine-DNA), 5′-(C6 amine)-TAA CAG GAT TAG CAG AGC GAG G-3′; Q-DNA, 5′-GCT AAT CCT GTT A-(BHQ2)-3′; T-DNA, 5′-CCT CGC TCT GCT AAT CCT GTT A-3′; single mismatch, 5′-CCT AGC TCT GCT AAT CCT GTT A-3′; three mismatches, 5′-CCT AGA TAT GCT AAT CCT GTT A-3′; five mismatches, 5′-CCT AGA TAT AAT AAT CCT GTT A-3′. Carboxyl-functionalized PS particles (80 nm in diameter, 2.5% w/v) were purchased from Spherotech. Cyanine 3 (Cy3) and amino-modified cyanine 3 (amine-Cy3) were purchased from Lumiprobe. 1-Ethyl-3(-3-dimethylaminopropyl) carbodiimide hydrochloride (EDC) was purchased from Sigma-Aldrich. Phosphate-buffered saline (PBS 1×, 140 mM NaCl, 2.7 mM KCl, 10 mM phosphate buffer, pH = 7.4) was purchased from Takara. Dimethyl sulfoxide (DMSO, ≥99.7%) and *N*,*N*-dimethylformamide (DMF, 99.8%) were purchased from Merck.

**Scheme 1. Schematic Representation of Fluorescent Nanoparticle-Based Nucleic Acid Detection. DNA-Immobilized Fluorescent PS Nanoparticles Are Prepared via Surface Reactions. Q-DNAs Are Hybridized to the Capture DNAs to Achieve the Off State of the Probe. T-DNAs Are Detected by Strand Displacement Resulting in the On State of the Probe**

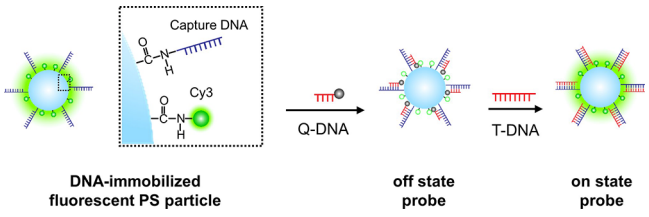


**Preparation of DNA-Immobilized Fluorescent PS Nanoparticles (PS@Cy3/DNA).** To covalently immobilize capture DNAs and fluorescent dyes on PS nanoparticle surfaces, amine-DNA and amine-Cy3 were used. In a typical experiment, 100 μL carboxylate PS particles (2.5% w/v) were dispersed in 900 μL of 1× PBS buffer solution. The PS particles were washed using 1× PBS, collected by centrifugation (Eppendorf, 13,200 rpm), and resuspended in 1 mL PBS. The carboxyl groups were activated by adding 0.5 mg of EDC into the PS particle solution. Amine-Cy3 and amine-DNA of desired molar concentrations were added to the activated PS particle solution. The solution was vortexed and incubated for 1 h, followed by the addition of 0.5 mg EDC. The mixture was kept in the dark at room temperature and reacted for 72 h under vigorous stirring. The resulting nanoparticles were washed with 1× PBS buffer twice then collected by centrifugation at 13,200 rpm. After the washing steps, the DNA content of the supernatant was measured using NanoDrop (Thermo Scientific) to confirm the absence of any unreacted oligonucleotides. The purified pellet was resuspended in 1 mL of 1× PBS buffer solution and kept in the dark until further use.

A control nanoparticle system was also prepared where the fluorescent dyes were fixed onto the PS particles by physical adsorption. Non-modified Cy3 (4.93 mg) was dispersed in 10 mL DMSO then diluted 10-fold. 50 μL of the Cy3 solution was combined with 1 mL of PS particles in PBS buffer. The mixture was vigorously stirred in the dark at room temperature for 72 h. The resulting nanoparticles were washed with 1× PBS buffer, then collected by centrifuge at 13,200 rpm. The purified pellet was resuspended in 1 mL of 1× PBS buffer solution. 0.5 mg of EDC was added to the suspension, followed by the addition of 50 μL of 100 μM amine-DNA. The solution was


https://doi.org/10.1021/acsomega.2c06498
ACS Omega 2022, 7, 48310−48319

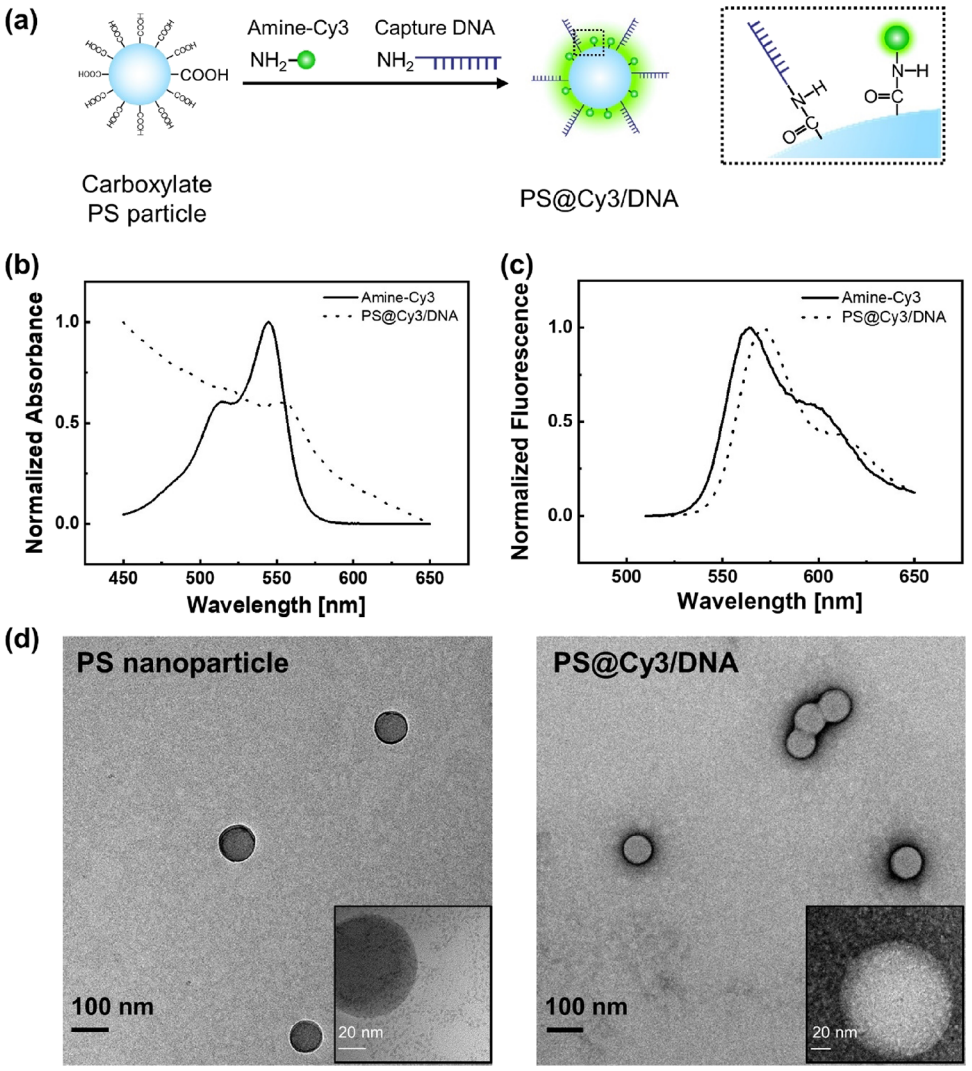


**Figure 1.** (a) Schematic of PS@Cy3/DNA preparation involving a simple one-pot reaction of incubating carboxylate PS nanoparticles in a solution of amine-Cy3 and amine-DNA. (b) Normalized absorbance spectra of amine-Cy3 (solid line) and PS@Cy3/DNA (dotted line). (c) Normalized fluorescence spectra of amine-Cy3 (solid line) and PS@Cy3/DNA (dotted line). (d) TEM images of bare PS nanoparticles and PS@Cy3/DNA nanoparticles. Higher-magnification images are shown in the insets. All samples are stained with 2% uranyl acetate.

vortexed and incubated for 1 h, followed by the addition of 0.5 mg of EDC. The mixture was stirred for 72 h at room temperature in the dark. The recovery of the particles followed the same procedure as described above.

**Preparation of Nanoprobe for T-DNA Detection.** PS@Cy3/DNA nanoparticles with desired dye and DNA content were prepared as described above. The off state of the probe was achieved by hybridizing the immobilized capture DNAs with Q-DNAs. Excess amounts of Q-DNAs were added to 100 $\mu$L of PS@Cy3/DNA nanoparticle solution. Q-DNA hybridization was conducted by heating the mixture to 95 °C for 3 min then cooling at a rate of −0.5 °C/min to 10 °C in a Thermomixer (Eppendorf). Unbound Q-DNAs were removed by washing at least twice. The nanoparticles were collected by centrifuge at 13,200 rpm, then redispersed in 100 $\mu$L PBS buffer. To estimate the Q-DNA hybridization efficiency, the nanoparticles were treated at a high temperature of 95 °C for 15 min. The eluted Q-DNAs were collected via centrifugation and quantified using NanoDrop.

For T-DNA detection, the probes in their off state were incubated with T-DNAs by heating to 95 °C for 3 min then cooling at a rate of −0.5 °C/min to 10 °C in a Thermomixer. The mixture was diluted 10-fold, then the fluorescence was determined by using a microplate reader.

**Characterization.** Transmission electron microscopy (TEM) was used to examine PS@Cy3/DNA nanoparticles. The TEM instrument (Tecnai F20) was operated at 200 kV. To prepare the sample grid, 12 $\mu$L of the sample nanoparticle solution was deposited onto a 200-mesh carbon-coated copper grid (Electron Microscopy Sciences) for 5 min, and the excess solution was wicked away with Whatman paper. Subsequently, the sample grid was treated with a 2% uranyl acetate staining solution for 2 min. The excess solution was wicked away and then dried by air before the examination. The absorbance spectra of the PS@Cy3/DNA nanoparticles were measured using a spectrophotometer (UV−visible/Near-Infrared spectrophotometer, Lambda 1050). The spectrum progressed from 300 to 800 nm at a 1 nm interval. Before sample measurements, the background was measured and subtracted. The fluorescence spectra of the PS@ Cy3/DNA nanoparticles were performed using a fluorometer (QM-400). For the standard recording of the fluorescence spectrum, the excitation


https://doi.org/10.1021/acsomega.2c06498
ACS Omega 2022, 7, 48310−48319

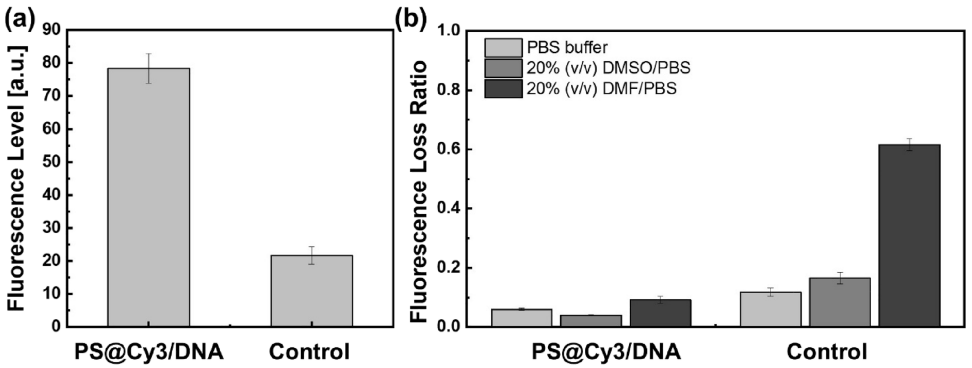


**Figure 2.** (a) Fluorescence intensity of PS@Cy3/DNA and control nanoparticles; both prepared at an input DNA concentration of 5 $\mu$M and dye concentration of 5 $\mu$M. (b) Fluorescence loss ratio, calculated by dividing the fluorescence of the residual solvent by the initial fluorescence of the nanoparticles for PS@Cy3/DNA and control nanoparticles following incubation in different solvent systems: PBS buffer, 20% (v/v) DMSO/PBS, and 20% (v/v) DMF/PBS. All samples are prepared in triplicate, and the average values are reported with standard deviations indicated as error bars.

wavelength was set to 488 nm. The slit size of the fluorometer was fixed to 2 nm, and the emission spectrum was measured from 500 to 800 nm at a 1 nm interval. The quantum yields (QYs) of the PS@Cy3/DNA nanoparticles were measured by using a QY spectrometer (Hamamatsu) equipped with an integrating sphere. For each measurement, the nanoparticle sample was transferred to a 1 cm quartz cuvette, and the excitation wavelength was set to 488 nm. The averaged absorbance and fluorescence intensities for the PS@Cy3/DNA nanoparticles and the nanoparticle-based probes were determined using a microplate reader (Varioskan LUX Multimode Microplate Reader, Thermo Fisher). The absorbance measurements were obtained at 545 nm. The fluorescence measurements were obtained with excitation and emission wavelengths of 550 and 570 nm, respectively.

## RESULTS AND DISCUSSION

**DNA-Immobilized Fluorescent PS Nanoparticles.** At the core of our design are PS nanoparticles immobilized with Cy3 dyes and capture DNA strands (PS@Cy3/DNA). We utilized 80 nm PS nanoparticles with surface carboxylic acid groups. Both the Cy3 dyes and the capture DNA sequences were designed to contain amine end groups; thus, they were covalently immobilized on PS nanoparticle surfaces via EDC-assisted coupling chemistry. As the addition sequence of amine-Cy3 and amine-DNA may affect their immobilization efficiency, we prepared three separate batches of nanoparticles at a fixed amine-DNA concentration of 5 $\mu$M and amine-Cy3 concentration of 5 $\mu$M but by following different addition orders: (1) amine-Cy3 first, then amine-DNA; (2) amine-DNA first, then amine-Cy3; and (3) simultaneous addition of amine-Cy3 and amine-DNA. The detailed synthesis procedures are described in Supplementary Information and Figure S1. For each batch of nanoparticles, we quantified the number of immobilized DNA and Cy3. The number of immobilized DNAs was determined by measuring the residual DNA concentration in the supernatant following nanoparticle recovery. The number of immobilized Cy3 dyes was determined by measuring the absorbance intensity at 545 nm of the same supernatant solution then correlating the measurement to the Cy3 concentration by applying a standard curve (Figure S2). Regardless of the addition order, the PS@Cy3/DNA nanoparticles prepared contained ~281 Cy3 dyes and ~115 DNA strands per particle, which translated to an immobilization efficiency of ~84% dyes and ~34% DNAs, respectively. The detailed immobilization efficiency data for the nanoparticles prepared following different addition methods are shown in Table S1.

As the addition sequence had minimal effect on the immobilization efficiency, we proceeded to prepare PS@Cy3/DNA nanoparticles by method (3), where the PS nanoparticles were simply incubated in a solution containing both amine-Cy3 and amine-DNA (Figure 1a). The successful incorporation of the dyes onto the PS nanoparticles was confirmed by spectroscopy measurements. The absorbance and fluorescence spectra of amine-Cy3 showed a red shift in maximum absorbance and fluorescence following immobilization on PS nanoparticles (Figure 1b,c). Note that in the absorbance spectra, the increased absorbance observed in the short-wavelength region was due to PS particle scattering.[38] The PS@Cy3/DNA nanoparticles were also examined by TEM, with representative images shown in Figure 1d. In comparison to the bare PS nanoparticles, the presence of DNA strands on PS@Cy3/DNA nanoparticles was clearly observed. Additionally, the PS@Cy3/DNA nanoparticles were confirmed to retain the spherical shape with low particle-to-particle aggregation.

The PS@Cy3/DNA nanoparticles were further examined for their optical properties and stability and compared to a control nanoparticle system where the dyes were fixed by physical adsorption. The control was prepared by using non-modified Cy3, and the dyes were physically fixed onto the PS nanoparticles via hydrophobic interaction. Amine-DNAs were still utilized as the capture DNAs, and they were immobilized on the particle surfaces via the same EDC-assisted coupling chemistry. The control system, prepared at an input DNA concentration of 5 $\mu$M and dye concentration of 5 $\mu$M, was determined to contain 81 $\pm$ 9 DNAs and 103 $\pm$ 2 dyes per particle. In comparison, the PS@Cy3/DNA nanoparticles prepared at the same DNA and dye concentrations had a DNA content of 112 $\pm$ 6 strands/particle and a much higher dye content of 306.4 $\pm$ 0.3 dyes/particle. The large difference in the number of dyes incorporated was supported by direct fluorescence measurements. As shown in Figure 2a, the PS@Cy3/DNA nanoparticles exhibit almost fourfold higher fluorescence intensity than the control nanoparticles. The stability of the PS@Cy3/DNA nanoparticles was examined by tracking dye release in different solvent conditions. The elution


https://doi.org/10.1021/acsomega.2c06498
ACS Omega 2022, 7, 48310−48319

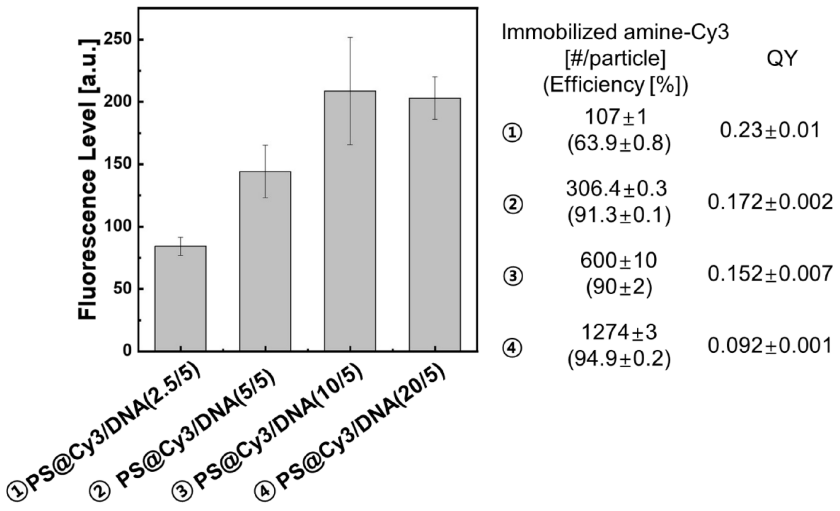


**Figure 3.** Fluorescence intensity for PS@Cy3/DNA nanoparticles prepared at a fixed amine-DNA concentration of 5 $\mu$M but varying amine-Cy3 concentrations of 2.5, 5, 10, and 20 $\mu$M. The calculated number of immobilized amine-Cy3 per nanoparticle, immobilization efficiency, and QY for each nanoparticle system are also indicated. All samples are prepared in triplicate, and the average values are reported with standard deviations.

of dye molecules is a critical concern when dye-immobilized nanoparticles are used as biosensors.[39,40] The loss of dye molecules lowers the sensor performance over time, and the released dyes are directly related to cytotoxicity issues.[41] We examined the elution of dye molecules from PS@Cy3/DNA in PBS buffer, 20% (v/v) DMSO/PBS mixture, and 20% (v/v) DMF/PBS mixture. The PBS buffer is chosen because it is the most common solvent for NA detection. The mixed solvents are used because DMSO and DMF are both good solvents for Cy3 and can thus serve as better indicators for the removal of loosely bound Cy3 dyes. The nanoparticles were stirred in the different solvents for 5 h under dark conditions, then the loss of dyes was determined by measuring the fluorescence of the residual solvents after nanoparticle recovery. Figure 2b shows the fluorescence loss ratio, calculated by dividing the measured solvent fluorescence by the initial fluorescence of the nanoparticle system. In comparison to the control, which showed high fluorescence loss, especially in the DMF/PBS mixture, the PS@Cy3/DNA nanoparticles showed small fluorescence loss with values of less than 0.1 in all solvent systems, indicating negligible dye losses. Collectively, the characterization data confirm that the PS@Cy3/DNA nanoparticles prepared by covalent immobilization of both capture DNAs and dyes show high fluorescence and stability, thus suitable for further probe development.

**Nanoprobe Preparation and Characterization.** To utilize the PS@Cy3/DNA nanoparticles as probes for T-DNA detection, we proceeded to optimize the fluorescence of the nanoparticles by tuning the number of immobilized Cy3 dyes. Different nanoparticles were prepared at a fixed amine-DNA molar concentration of 5 $\mu$M and varying amine-Cy3 molar concentrations in the range of 2.5 to 20 $\mu$M. The resulting nanoparticles were designated as PS@Cy3/DNA($X$/$Y$), where X and Y denoted the input molar concentration of amine-Cy3 and amine-DNA, respectively. The number of Cy3 immobilized was measured, and the values increased from 107 dyes/particle to 1274 dyes/particle as the input amine-Cy3 concentration increased. The fluorescence intensity exhibited by each nanoparticle system is shown in Figure 3. An increase in the fluorescence was confirmed initially; however, as the amine-Cy3 concentration reached over 10 $\mu$M, a further increase in the dye concentration did not lead to an additional increase in nanoparticle fluorescence. We attribute the observed plateau in nanoparticle fluorescence to dye aggregation-induced self-quenching at high concentrations.[40] This conclusion was also supported by QY measurements. For the four nanoparticle systems prepared with increasing dye concentrations, their measured QY values decreased in the order of 0.23 (PS@Cy3/DNA(2.5/5)), 0.172 (PS@Cy3/DNA(5/5)), 0.152 (PS@Cy3/DNA(10/5)), and 0.092 (PS@Cy3/DNA(20/5)). Taking into consideration both the overall fluorescence and the QY, we chose to prepare the nanoprobes by fixing the dye concentration at 5 $\mu$M.

For the operation of the nanoparticles as DNA probes, we followed a strand displacement strategy in which the off state of the probe was prepared by hybridizing Q-DNA sequences to the capture DNAs on the nanoparticles. The short Q-DNAs have a lower affinity to the capture DNAs than the longer T-DNAs. Thus, in the presence of T-DNAs, binding between the T-DNAs and the capture DNAs displaces the prehybridized Q-DNAs, leading to the detection of the T-DNAs as indicated by an increase in the nanoparticle fluorescence. This strategy has the advantage of showing high specificity to target species with negligible response to non-targets when the sensors undergo any chemical or physical changes.[42−44] Additionally, the use of Q-DNA to quench nanoparticle fluorescence eliminates the need to modify T-DNA, which can be time-consuming yet far less efficient.[42,45]

We utilized a 13 mer DNA sequence with a blackhole quencher 2 (BHQ2) attached to its 3′ end as the Q-DNA for nanoprobe preparation in this study. As illustrated in Figure 4, following the hybridization of Q-DNAs and the capture DNAs on PS@Cy3/DNA, the BHQ2 ends of the Q-DNAs are placed in close proximity to the Cy3 dyes immobilized on the PS surfaces. The fluorescence intensity of the nanoparticles is then effectively quenched, giving the desired off state of the probes. The number of Q-DNAs required to effectively quench the fluorescence of the nanoparticles was examined by hybridizing PS@Cy3/DNA(5/5) with excess Q-DNAs relative to the input capture DNAs. In comparison to the nanoparticles with no Q-DNAs, a drop in the fluorescence intensity by ∼37% is observed, as shown in Figure 4. We further quantified the


https://doi.org/10.1021/acsomega.2c06498
ACS Omega 2022, 7, 48310−48319

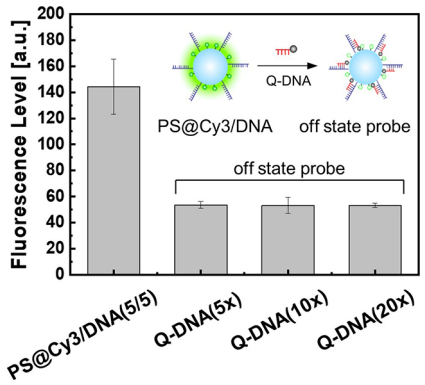


**Figure 4.** Fluorescence intensity for PS@Cy3/DNA(5/5) nanoparticles before and after hybridizing with 5×, 10×, and 20× excess of Q-DNAs. All samples are prepared in triplicate, and the average values are reported with standard deviations indicated as error bars. A schematic for the preparation of the probe's off state by hybridizing Q-DNAs with the capture DNAs on PS@Cy3/DNA is also shown.

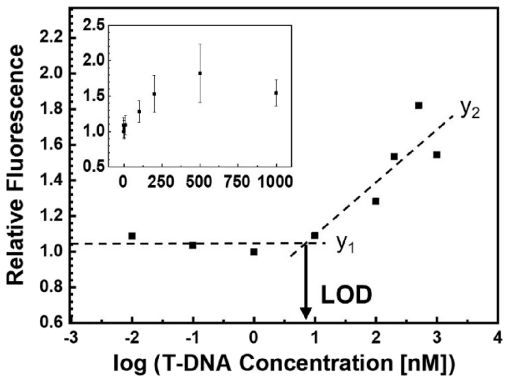


**Figure 5.** Semi-log plot of relative fluorescence of Q-DNA-prehybridized PS@Cy3/DNA(5/5) nanoprobes as a function of T-DNA concentrations. At low T-DNA concentrations, the detection profile is represented by a flat line: $y_1 = 1.04$. At high T-DNA concentrations, the detection profile is represented by a best-fit linear function: $y_2 = 0.31x + 0.78$. The LOD is defined as the intersection of the two functions. The same plot in the linear scale is shown in the inset. The fluorescence measurements are repeated three times, and the average values are reported with standard deviations indicated as error bars.

hybridization efficiency between the Q-DNAs and the capture DNAs by heating the nanoparticles to 95 °C to induce dehybridization of any double-stranded DNAs. By tracking the amount of the eluted Q-DNAs, the hybridization efficiency was estimated to be 32, 57, and 55% for systems prepared at 5×, 10×, and 20× excess Q-DNAs, respectively. As the on state of the probe is triggered by displacing the Q-DNAs with T-DNA binding, a high hybridization efficiency between the Q-DNAs and the capture DNAs in the off state is beneficial. Therefore, we find that the off state prepared at 10× excess Q-DNA concentration shows both reasonable hybridization efficiency and sufficient decrease in fluorescence, thus suitable for nanoprobe operation.

The nanoprobes thus prepared were tested for T-DNA detection. The T-DNA sequence chosen in this study is a part of the plasmid cloning vector in *Escherichia coli*, widely used as a model target for biosensing applications.[46,47] The PS@Cy3/DNA(5/5) nanoparticles were first synthesized by mixing PS nanoparticles in a solution of 5 $\mu$M amine-Cy3 and 5 $\mu$M amine-DNA. The nanoparticles were then hybridized with 10× excess of Q-DNAs to achieve the off state. The Q-DNA-prehybridized nanoparticles then served as probes, and they were incubated in T-DNA-containing buffer solutions. The detection profile was constructed by tracking the increase in solution fluorescence. We tested the nanoprobes in T-DNA solutions in the concentration range from $1 \times 10^{-2}$ to $1 \times 10^{3}$ nM, and a typical detection profile is shown in Figure 5. The data are presented in relative fluorescence, and the values are calculated by normalizing the measured solution fluorescence intensities against the fluorescence exhibited by the nanoprobes in the off state. At low T-DNA concentrations, the fluorescence remained low and the detection profile was represented by a flat line ($y_1$) with the value of the average relative fluorescence in the region. At high T-DNA concentrations passing a threshold value, an increase in the log-scale fluorescence was observed and the detection profile was represented by a best-fit linear function ($y_2$). We defined the intersection of $y_1$ and $y_2$ as the limit of detection (LOD) for the nanoprobe. For the detection profile shown in Figure 5, the calculated LOD was 7.2 nM. As the sample volume was 100 $\mu$L, the probes can detect T-DNA as low as $7.2 \times 10^{2}$ fmol. This result indicates that the probes developed are capable of detecting T-DNAs with high sensitivity comparable to previously reported particle-based detection platforms summarized in Table S2.

The performance of the probe was further evaluated in terms of sequence specificity and long-term stability. The detection specificity was examined by testing the Q-DNA-prehybridized PS@Cy3/DNA(5/5) probes against DNA sequences containing different numbers of mismatches. As shown in Figure 6a, the probes responded with a high fluorescence increase to the T-DNA sequence. However, the detected fluorescence intensity dropped significantly when the target-competitive sequence contained a single mismatch (mismatch 1) located at the fourth position from the 5′ end. The sequences containing three (mismatch 3) and five mismatches (mismatch 5) further deteriorated the fluorescence response from the probes, and the measured fluorescence intensities became indistinguishable from the probes' off state. The results indicate that the developed PS@Cy3/DNA-based nanoprobes can be used to detect T-DNA in a mixture of similar DNA sequences with high specificity. The operation lifetime of the probe was evaluated by tracking its performance for a 2-month period. Organic dyes are known to show a steady decrease in the fluorescence signal.[48] Their photostability is also influenced by multiple factors, including light exposure, chemical alternation, and oxygen in the surrounding environment.[31,49] Thus, it is important to determine the time period over which the developed probes can maintain the fluorescence signal. We tracked the fluorescence exhibited by the probes in the off state and on state in response to T-DNA from the day the probes were synthesized (day 1) up to 2 months at a 2-week interval, and the results are summarized in Figure 6b. The fluorescence level exhibited by the probes in their on state remained consistently high for 1 month then decreased after the period. We note that after 1 month, although the overall fluorescence of the probes decreased, detection of the T-DNA can still be performed, given that the intensity difference between the on and off states was reduced. Similar stability performances were also reported by other DNA-immobilized dye-loaded polymeric nanoparticle systems.[10]


https://doi.org/10.1021/acsomega.2c06498
ACS Omega 2022, 7, 48310−48319

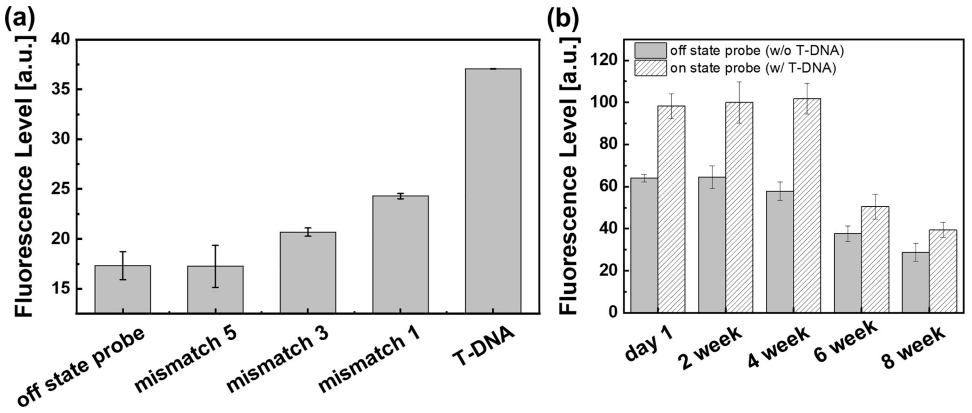


**Figure 6.** (a) Sequence specificity of the Q-DNA-prehybridized PS@Cy3/DNA(5/5) nanoprobes. The fluorescence responses of the nanoprobes after incubating in solutions containing T-DNA and DNA sequences with one, three, and five mismatches are compared to the fluorescence of the probes in the off state. (b) Lifetime evaluation of the Q-DNA-prehybridized PS@Cy3/DNA(5/5) nanoprobes. The fluorescence intensities of the nanoprobes in the off state and on state in response to T-DNA are compared over 8 weeks at a 2-week interval. All samples are prepared in triplicate, and the average values are reported with standard deviations indicated as error bars.

**Table 1. Characterization of PS@Cy3/DNA Nanoparticles Prepared at a Fixed Amine-Cy3 Concentration of 5 $\mu$M and Varied Amine-DNA Concentrations of 2.5, 5, 10, and 20 $\mu$M**

| | immobilized amine-Cy3[a,b] | | immobilized amine-DNA[a,c] | | |
|---|---|---|---|---|---|
| PS@Cy3/DNA (Cy3/DNA $\mu$M) | [#/particle] | efficiency [%] | [#/particle] | efficiency [%] | QY[a] |
| (5/2.5) | 295.6 ± 0.6 | 88.1 ± 0.2 | 33 ± 1 | 19 ± 1 | 0.190 ± 0.003 |
| (5/5) | 306.4 ± 0.3 | 91.3 ± 0.1 | 112 ± 6 | 34 ± 2 | 0.172 ± 0.002 |
| (5/10) | 307.0 ± 0.1 | 91.49 ± 0.02 | 210 ± 20 | 31 ± 3 | 0.228 ± 0.006 |
| (5/20) | 310 ± 2 | 92.2 ± 0.7 | 350 ± 50 | 26 ± 4 | 0.165 ± 0.004 |

[a]Samples are prepared in triplicate, and the average values are reported with standard deviations. [b]Determined by measuring the absorbance intensity at 545 nm of the supernatant solution following nanoparticle recovery, then correlating the measurement to Cy3 concentration by applying a standard curve. [c]Determined by measuring the residual DNA concentration in the supernatant solution.

**Tuning Nanoprobe Detection Limit.** While many biosensors have been reported over the years, most of them are optimized to exhibit a single detection profile with a fixed LOD value and the ability to prepare sensors with tunable LOD is often overlooked. Such capability can be important to many biomedical applications, which require the detection of biomolecules when they are present above different critical concentrations.[50−52] The PS@Cy3/DNA-based nanoprobes reported in this study use surface chemistry such that the number of immobilized capture DNAs and dyes can be independently tuned by controlling the input concentrations of amine-DNA and amine-Cy3. We envision that PS@Cy3/DNA nanoparticles containing different ratios of capture DNAs to dyes can be prepared, and the corresponding nanoprobes are expected to show different LOD values in response to T-DNAs. To prepare PS@Cy3/DNA nanoparticles with different capture DNA-to-dye ratios, we fixed the amine-Cy3 concentration at 5 $\mu$M and varied the amine-DNA concentration in the range of 2.5 to 20 $\mu$M. Four different types of PS@Cy3/DNA nanoparticles were prepared, and the number of immobilized Cy3 dyes and DNAs for each nanoparticle system were quantified and are reported in Table 1. As the amine-Cy3 concentration was fixed, the number of dyes immobilized was similar at around 305 dyes/particle for all four types of nanoparticles. The values were also consistent with the number of immobilized dyes reported earlier (see Table S1). The increasing concentration of input amine-DNA led to an increase in the number of immobilized DNA from 33 ± 1 to 350 ± 50 strands per particle, thus confirming the successful preparation of PS@Cy3/DNA nanoparticles with an increasing capture DNA-to-dye ratio. We further measured the QYs for the four nanoparticle systems. As shown in Table 1, all four systems had QYs at around 0.19, indicating that the increase in surface immobilized capture DNA density had a negligible effect on dye quenching.

The prepared PS@Cy3/DNA nanoparticles were then hybridized with 10× Q-DNAs following the previously described procedures to prepare the nanoprobes for T-DNA detection. The representative detection profile of the nanoprobes made using PS@Cy3/DNA(5/2.5) and PS@Cy3/DNA(5/10) is shown in Figure 7a and 7b, respectively (detection profile of PS@Cy3/DNA(5/5)-based nanoprobes is shown in Figure 5). To determine the reproducibility of the obtained detection profiles, each nanoprobe system was tested two to three times, and the additional detection profiles are detailed in Figures S3−S5. The LOD values for the nanoprobes were also calculated based on their detection profiles, and the averaged values were 2.6 nM for PS@Cy3/DNA (5/2.5), 8.3 nM for PS@Cy3/DNA(5/5), and 22.3 nM for PS@Cy3/DNA (5/10), as illustrated in Figure 7c. The detection profiles for PS@Cy3/DNA(5/20)-based nanoprobes were also obtained and shown in Figure S6. In this case, LOD could not be determined as the detection profiles showed no discrimination in the relative fluorescence over a wide T-DNA concentration range. The results verified our initial hypothesis and confirmed that the LOD values of the PS@Cy3/DNA-based nanoprobes could indeed be increased as the surface immobilized capture DNA-to-dye ratio increased. Assuming all PS@Cy3/DNA nanoparticles exhibit similar hybridization efficiency with Q-DNAs, an increase in the capture DNA-to-


https://doi.org/10.1021/acsomega.2c06498
ACS Omega 2022, 7, 48310−48319

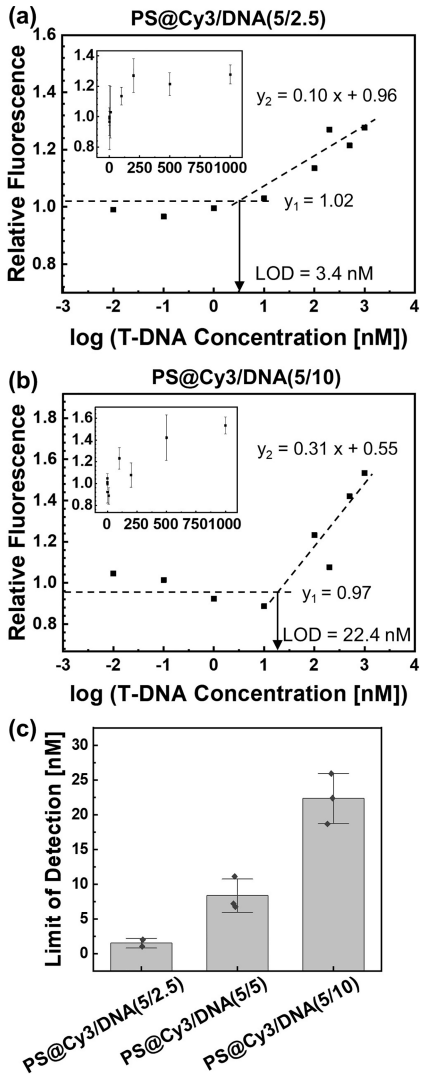


**Figure 7.** Semi-log plot of relative fluorescence of nanoprobes prepared using (a) PS@Cy3/DNA(5/2.5) and (b) PS@Cy3/DNA(5/10) as a function of T-DNA concentrations. At low T-DNA concentrations, the detection profile is modeled by $y_1$. At high T-DNA concentrations, the detection profile is modeled by $y_2$. The LOD is defined as the intersection of $y_1$ and $y_2$. The corresponding plots in the linear scale are shown in the insets. All fluorescence measurements are repeated three times, and the average values are reported with standard deviations indicated as error bars. (c) Calculated LOD values for PS@Cy3/DNA-based nanoprobes, prepared at different amine-DNA to amine-Cy3 input concentrations. The LOD values calculated from each detection experiment are indicated by the solid diamond symbols. The bar graph represents the averaged LOD values with standard deviation shown as error bars.

dye ratio would then increase the number of hybridized Q-DNAs present in the off state of the nanoprobes. When the probes are incubated with T-DNAs, a correspondingly higher number of T-DNAs would be required to displace the Q-DNAs, leading to the observed increase in LOD. It is also interesting to note that the slope of the linearly increasing region ($y_2$) of the detection profile increased from 0.10 to 0.34 as the capture DNA-to-dye ratio increased. We speculate that with a higher density of capture DNAs and consequently higher density of Q-DNAs on the nanoparticle surfaces, the quenching efficiency of the nanoprobes in the off state may be improved,[53] leading to an increased signal-to-background ratio as reflected by a steeper fluorescence increase in the $y_2$ region of the detection profile.

## CONCLUSION

In this study, PS@Cy3/DNA nanoparticles were prepared by reacting carboxyl-functionalized PS nanoparticles with amine-functionalized capture DNAs and dye molecules. The numbers of immobilized capture DNAs and Cy3 dyes were quantified, and they were well correlated with the initial concentrations of amine-DNA and amine-Cy3 used for nanoparticle synthesis. The PS@Cy3/DNA nanoparticles showed high fluorescence and low dye leakage; thus, they were further utilized to construct nanoprobes for T-DNA detection. The off state of the nanoprobes was achieved by hybridizing short Q-DNA strands to the capture DNAs on PS@Cy3/DNA, and an optimized 10× excess Q-DNA relative to the initial input amine-DNA concentration was determined to produce the desired probe off state with sufficiently reduced fluorescence and reasonable hybridization efficiency. The Q-DNA-prehybridized PS@Cy3/DNA nanoprobes were then successfully employed to detect T-DNA via a strand displacement strategy. We verified that the probes could detect T-DNA with high sequence specificity, and they maintained an operation lifetime comparable to other dye-loaded polymeric particles. The detection profiles of the nanoprobes were also investigated. We showed that the probes exhibited a low detection limit in the femto-mole range, and the LOD value could be tuned by adjusting the surface immobilized capture DNA-to-dye ratios. Specifically, when the capture DNA-to-dye ratio increased, the LOD of the nanoprobes also increased due to the increasing amount of Q-DNAs required to be displaced to achieve the on state. Overall, we systematically investigated organic DNA probes constructed using PS@Cy3/DNA nanoparticles. The well-controlled surface chemistry rendered the prepared probes to show high sensitivity and stability, thus having the potential to be used for various in vitro and in vivo bio-imaging and biosensing applications. Furthermore, the detection profile of the nanoprobes can be tuned, which can provide the design basis of biosensors with tailored LOD for the detection of biomolecules above different critical concentrations.

## ASSOCIATED CONTENT

### Supporting Information

The Supporting Information is available free of charge at https://pubs.acs.org/doi/10.1021/acsomega.2c06498.

Additional experimental details and characterization of PS@Cy3/DNA via different addition methods; calibration curve for dye concentration measurement; reported particle-based biosensor LOD values; additional detection profiles of PS@Cy3/DNA-based nanoprobes (PDF)

## AUTHOR INFORMATION

### Corresponding Author

**Sheng Li** − *Department of Chemical and Biomolecular Engineering, Korea Advanced Institute of Science and Technology (KAIST), Daejeon 34141, Republic of Korea;* orcid.org/0000-0002-6172-5705; Phone: +82-42-350-7313; Email: shengli@kaist.ac.kr



https://doi.org/10.1021/acsomega.2c06498
*ACS Omega* 2022, 7, 48310−48319

### Author

**Jin Sol Shin** − *Department of Chemical and Biomolecular Engineering, Korea Advanced Institute of Science and Technology (KAIST), Daejeon 34141, Republic of Korea*

Complete contact information is available at: https://pubs.acs.org/10.1021/acsomega.2c06498


### Notes

The authors declare no competing financial interest.

## ■ ACKNOWLEDGMENTS

This work was supported by the Korean Government Ministry of Science and ICT (NRF-2020R1C1C1007291).

## ■ REFERENCES


(1) Suea-Ngam, A.; Bezinge, L.; Mateescu, B.; Howes, P. D.; deMello, A. J.; Richards, D. A. Enzyme-Assisted Nucleic Acid Detection for Infectious Disease Diagnostics: Moving Toward the Point-of-Care. *ACS Sens.* **2020**, *5*, 2701−2723.

(2) Du, Y.; Pothukuchy, A.; Gollihar, J. D.; Nourani, A.; Li, B.; Ellington, A. D. Coupling Sensitive Nucleic Acid Amplification with Commercial Pregnancy Test Strips. *Angew. Chem., Int. Ed. Engl.* **2017**, *56*, 992−996.

(3) Marras, S. A.; Kramer, F. R.; Tyagi, S. Efficiencies of Fluorescence Resonance Energy Transfer and Contact-Mediated Quenching in Oligonucleotide Probes. *Nucleic Acids Res.* **2002**, *30*, 122e.

(4) Ashe, S.; Maji, U. J.; Sen, R.; Mohanty, S.; Maiti, N. K. Specific Oligonucleotide Primers for Detection of Endoglucanase Positive *Bacillus subtilis* by PCR. *Biotech* **2014**, *4*, 461−465.

(5) Gore, H. M.; Wakeman, C. A.; Hull, R. M.; McKillip, J. L. Real-Time Molecular Beacon NASBA Reveals hblC Expression from *Bacillus spp.* in Milk. *Biochem. Biophys. Res. Commun.* **2003**, *311*, 386−390.

(6) Chen, L.; Song, L.; Zhang, Y.; Wang, P.; Xiao, Z.; Guo, Y.; Cao, F. Nitrogen and Sulfur Codoped Reduced Graphene Oxide as a General Platform for Rapid and Sensitive Fluorescent Detection of Biological Species. *ACS Appl. Mater. Interfaces* **2016**, *8*, 11255−11261.

(7) Zhao, Q.; Piao, J.; Peng, W.; Wang, Y.; Zhang, B.; Gong, X.; Chang, J. Simple and Sensitive Quantification of MicroRNAs via PS@Au Microspheres-Based DNA Probes and DSN-Assisted Signal Amplification Platform. *ACS Appl. Mater. Interfaces* **2018**, *10*, 3324−3332.

(8) Thomson, D. A. C.; Dimitrov, K.; Cooper, M. A. Amplification Free Detection of Herpes Simplex Virus DNA. *Analyst* **2011**, *136*, 1599−1607.

(9) Qiu, X.; Hildebrandt, N. Rapid and Multiplexed MicroRNA Diagnostic Assay Using Quantum Dot-Based Förster Resonance Energy Transfer. *ACS Nano* **2015**, *9*, 8449−8457.

(10) Melnychuk, N.; Klymchenko, A. S. DNA-Functionalized Dye-Loaded Polymeric Nanoparticles: Ultrabright FRET Platform for Amplified Detection of Nucleic Acids. *J. Am. Chem. Soc.* **2018**, *140*, 10856−10865.

(11) Lu, W.; Chen, Y.; Liu, Z.; Tang, W.; Feng, Q.; Sun, J.; Jiang, X. Quantitative Detection of MicroRNA in One Step via Next Generation Magnetic Relaxation Switch Sensing. *ACS Nano* **2016**, *10*, 6685−6692.

(12) Pang, Y.; Wang, C.; Wang, J.; Sun, Z.; Xiao, R.; Wang, S. $Fe_3O_4$@Ag Magnetic Nanoparticles for MicroRNA Capture and Duplex-Specific Nuclease Signal Amplification Based SERS Detection in Cancer Cells. *Biosens. Bioelectron.* **2016**, *79*, 574−580.

(13) Yang, Y.; Huang, J.; Yang, X.; He, X.; Quan, K.; Xie, N.; Ou, M.; Wang, K. Gold Nanoparticle Based Hairpin-Locked-DNAzyme Probe for Amplified miRNA Imaging in Living Cells. *Anal. Chem.* **2017**, *89*, 5850−5856.

(14) Yang, Y.; Zhong, S.; Wang, K.; Huang, J. Gold Nanoparticle Based Fluorescent Oligonucleotide Probes for Imaging and Therapy in Living Systems. *Analyst* **2019**, *144*, 1052−1072.

(15) Rouge, J. L.; Hao, L.; Wu, X. A.; Briley, W. E.; Mirkin, C. A. Spherical Nucleic Acids as a Divergent Platform for Synthesizing RNA-Nanoparticle Conjugates Through Enzymatic Ligation. *ACS Nano* **2014**, *8*, 8837−8843.

(16) Sheng, W.; Wei, W.; Li, J.; Qi, X.; Zuo, G.; Chen, Q.; Pan, X.; Dong, W. Amine-Functionalized Magnetic Mesoporous Silica Nanoparticles for DNA Separation. *Appl. Surf. Sci.* **2016**, *387*, 1116−1124.

(17) Chen, J.; Luo, Z.; Wang, Y.; Huang, Z.; Li, Y.; Duan, Y. DNA Specificity Detection with High Discrimination Performance in Silver Nanoparticle Coupled Directional Fluorescence Spectrometry. *Sens. Actuators, B* **2018**, *255*, 2306−2313.

(18) Liu, Y.; Kannegulla, A.; Wu, B.; Cheng, L. J. Quantum Dot Fullerene-Based Molecular Beacon Nanosensors for Rapid, Highly Sensitive Nucleic Acid Detection. *ACS Appl. Mater. Interfaces* **2018**, *10*, 18524−18531.

(19) Ha, S.-W.; Weitzmann, M. N.; Beck, G. R., Jr. Bioactive Silica Nanoparticles Promote Osteoblast Differentiation Through Stimulation of Autophagy and Direct Association with LC3 and p62. *ACS Nano* **2014**, *8*, 5898−5910.

(20) Beck, G. R., Jr.; Ha, S. W.; Camalier, C. E.; Yamaguchi, M.; Li, Y.; Lee, J. K.; Weitzmann, M. N. Bioactive Silica-Based Nanoparticles Stimulate Bone-Forming Osteoblasts, Suppress Bone-Resorbing Osteoclasts, and Enhance Bone Mineral Density *in vivo*. *Nanomedicine* **2012**, *8*, 793−803.

(21) Gubala, V.; Giovannini, G.; Kunc, F.; Monopoli, M. P.; Moore, C. J. Dye-Doped Silica Nanoparticles: Synthesis, Surface Chemistry and Bioapplications. *Cancer Nanotechnol.* **2020**, *11*, 1.

(22) Dubertret, B.; Skourides, P.; Norris, D. J.; Noireaux, V.; Brivanlou, A. H.; Libchaber, A. *In vivo* Imaging of Quantum Dots Encapsulated in Phospholipid Micelles. *Science* **2002**, *298*, 1759−1762.

(23) Chueh, P. J.; Liang, R. Y.; Lee, Y. H.; Zeng, Z. M.; Chuang, S. M. Differential Cytotoxic Effects of Gold Nanoparticles in Different Mammalian Cell Lines. *J. Hazard. Mater.* **2014**, *264*, 303−312.

(24) Libralato, G.; Galdiero, E.; Falanga, A.; Carotenuto, R.; De Alteriis, E.; Guida, M. Toxicity Effects of Functionalized Quantum Dots, Gold and Polystyrene Nanoparticles on Target Aquatic Biological Models: A Review. *Molecules* **2017**, *22*, 1439.

(25) Cheng, S.; Li, A.; Pan, X.; Wang, H.; Zhang, C.; Li, J.; Qi, X. A Near-Infrared Fluorescent Probe for Highly Specific and Ultrasensitive Detection of Hypochlorite Ions in Living Cells. *Anal. Bioanal. Chem.* **2021**, *413*, 4441−4450.

(26) Pan, X.; Cheng, S.; Zhang, C.; Qi, X. Two Highly Sensitive Fluorescent Probes based on Cinnamaldehyde with Large Stokes Shift for Sensing of $HSO_3^{(-)}$ in Pure Water and Living Cells. *Anal. Bioanal. Chem.* **2020**, *412*, 6959−6968.

(27) Li, X.; Figg, C. A.; Wang, R.; Jiang, Y.; Lyu, Y.; Sun, H.; Liu, Y.; Wang, Y.; Teng, I. T.; Hou, W.; et al. Cross-Linked Aptamer-Lipid Micelles for Excellent Stability and Specificity in Target-Cell Recognition. *Angew. Chem., Int. Ed. Engl.* **2018**, *57*, 11589−11593.

(28) Wagh, A.; Qian, S. Y.; Law, B. Development of Biocompatible Polymeric Nanoparticles for *in vivo* NIR and FRET Imaging. *Bioconjugate Chem.* **2012**, *23*, 981−992.

(29) Wagh, A.; Jyoti, F.; Mallik, S.; Qian, S.; Leclerc, E.; Law, B. Polymeric Nanoparticles with Sequential and Multiple FRET Cascade Mechanisms for Multicolor and Multiplexed Imaging. *Small* **2013**, *9*, 2129−2139.

(30) Wang, X.; Groff, L. C.; McNeill, J. D. Photoactivation and Saturated Emission in Blended Conjugated Polymer Nanoparticles. *Langmuir* **2013**, *29*, 13925−13931.

(31) Reisch, A.; Klymchenko, A. S. Fluorescent Polymer Nanoparticles Based on Dyes: Seeking Brighter Tools for Bioimaging. *Small* **2016**, *12*, 1968−1992.

(32) Caputo, T. M.; Battista, E.; Netti, P. A.; Causa, F. Supramolecular Microgels with Molecular Beacons at the Interface for Ultrasensitive, Amplification-Free, and SNP-Selective miRNA

Fluorescence Detection. *ACS Appl. Mater. Interfaces* **2019**, *11*, 17147−17156.
(33) Stawicki, C. M.; Rinker, T. E.; Burns, M.; Tonapi, S. S.; Galimidi, R. P.; Anumala, D.; Robinson, J. K.; Klein, J. S.; Mallick, P. Modular Fluorescent Nanoparticle DNA Probes for Detection of Peptides and Proteins. *Sci. Rep.* **2021**, *11*, 19921.
(34) Visaveliya, N. R.; Köhler, J. M. Softness Meets with Brightness: Dye-Doped Multifunctional Fluorescent Polymer Particles via Microfluidics for Labeling. *Adv. Opt. Mater.* **2021**, *9*, 2002219.
(35) Kalelkar, P. P.; Collard, D. M. Tricomponent Amphiphilic Poly(oligo(ethylene glycol) methacrylate) Brush-Grafted Poly(lactic acid): Synthesis, Nanoparticle Formation, and *in vitro* Uptake and Release of Hydrophobic Dyes. *Macromolecules* **2020**, *53*, 4274−4283.
(36) Reisch, A.; Didier, P.; Richert, L.; Oncul, S.; Arntz, Y.; Mély, Y.; Klymchenko, A. S. Collective Fluorescence Switching of Counterion-Assembled Dyes in Polymer Nanoparticles. *Nat. Commun.* **2014**, *5*, 4089.
(37) Bilal, M.; Asgher, M.; Cheng, H.; Yan, Y.; Iqbal, H. M. N. Multi-Point Enzyme Immobilization, Surface Chemistry, and Novel Platforms: a Paradigm Shift in Biocatalyst Design. *Crit. Rev. Biotechnol.* **2019**, *39*, 202−219.
(38) Würth, C.; Grabolle, M.; Pauli, J.; Spieles, M.; Resch-Genger, U. Relative and Absolute Determination of Fluorescence Quantum Yields of Transparent Samples. *Nat. Protoc.* **2013**, *8*, 1535−1550.
(39) Tenuta, T.; Monopoli, M. P.; Kim, J.; Salvati, A.; Dawson, K. A.; Sandin, P.; Lynch, I. Elution of Labile Fluorescent Dye from Nanoparticles during Biological Use. *PLoS One* **2011**, *6*, No. e25556.
(40) Behnke, T.; Wurth, C.; Hoffmann, K.; Hübner, M.; Panne, U.; Resch-Genger, U. Encapsulation of Hydrophobic Dyes in Polystyrene Micro- and Nanoparticles via Swelling Procedures. *J. Fluoresc.* **2011**, *21*, 937−944.
(41) Pauli, J.; Vag, T.; Haag, R.; Spieles, M.; Wenzel, M.; Kaiser, W. A.; Resch-Genger, U.; Hilger, I. An *in vitro* Characterization Study of New Near Infrared Dyes for Molecular Imaging. *Eur. J. Med. Chem.* **2009**, *44*, 3496−3503.
(42) Gliddon, H. D.; Howes, P. D.; Kaforou, M.; Levin, M.; Stevens, M. M. A Nucleic Acid Strand Displacement System for the Multiplexed Detection of Tuberculosis-Specific mRNA using Quantum Dots. *Nanoscale* **2016**, *8*, 10087−10095.
(43) Phillips, E. A.; Moehling, T. J.; Bhadra, S.; Ellington, A. D.; Linnes, J. C. Strand Displacement Probes Combined with Isothermal Nucleic Acid Amplification for Instrument-Free Detection from Complex Samples. *Anal. Chem.* **2018**, *90*, 6580−6586.
(44) Larkey, N. E.; Almlie, C. K.; Tran, V.; Egan, M.; Burrows, S. M. Detection of miRNA using a Double-Strand Displacement Biosensor with a Self-Complementary Fluorescent Reporter. *Anal. Chem.* **2014**, *86*, 1853−1863.
(45) Liu, Y. H.; Tsai, Y. Y.; Chien, H. J.; Chen, C. Y.; Huang, Y. F.; Chen, J. S.; Wu, Y. C.; Chen, C. C. Quantum-Dot-Embedded Silica Nanotubes as Nanoprobes for Simple and Sensitive DNA Detection. *Nanotechnology* **2011**, *22*, No. 155102.
(46) Kwak, M.; Musser, A. J.; Lee, J.; Herrmann, A. DNA-Functionalised Blend Micelles: Mix and Fix Polymeric Hybrid Nanostructures. *Chem. Commun.* **2010**, *46*, 4935−4937.
(47) Kim, J. H.; Smit, J. H.; Prusty, D. K.; Musser, A. J.; Tombros, N.; Lee, P. C. W.; Herrmann, A.; Kwak, M. Ultrasensitive Detection of Oligonucleotides: Single-Walled Carbon Nanotube Transistor Assembled by DNA Block Copolymer. *J. Nanosci. Nanotechnol.* **2017**, *17*, 5175−5180.
(48) Demchenko, A. P. Photobleaching of Organic Fluorophores: Quantitative Characterization, Mechanisms, Protection. *Methods Appl. Fluoresc.* **2020**, *8*, No. 022001.
(49) Saxena, V.; Sadoqi, M.; Shao, J. Enhanced Photo-Stability, Thermal-Stability and Aqueous-Stability of Indocyanine Green in Polymeric Nanoparticulate Systems. *J. Photochem. Photobiol., B* **2004**, *74*, 29−38.
(50) Zhang, X.; Wang, Y.; Deng, H.; Xiong, X.; Zhang, H.; Liang, T.; Li, C. An Aptamer Biosensor for CA125 Quantification in Human Serum Based on Upconversion Luminescence Resonance Energy Transfer. *Microchem. J.* **2021**, *161*, No. 105761.
(51) Liang, Y.; Wang, W.; Fang, C.; Raj, S.-S.; Hu, W.-M.; Li, Q.-W.; Zhou, Z.-W. Clinical Significance and Diagnostic Value of Serum CEA, CA19-9 and CA72-4 in Patients with Gastric Cancer. *Oncotarget* **2016**, *7*, 49565−49573.
(52) Xu, Z.; Wang, C.; Ma, R.; Sha, Z.; Liang, F.; Sun, S. Aptamer-Based Biosensing Through the Mapping of Encoding Upconversion Nanoparticles for Sensitive CEA Detection. *Analyst* **2022**, *147*, 3350−3359.
(53) Yang, C. J.; Lin, H.; Tan, W. Molecular Assembly of Superquenchers in Signaling Molecular Interactions. *J. Am. Chem. Soc.* **2005**, *127*, 12772−12773.


https://doi.org/10.1021/acsomega.2c06498
*ACS Omega* 2022, 7, 48310−48319